Experimental Thermal and Fluid Science 150 (2024) 111046

Contents lists available at ScienceDirect

Experimental Thermal and Fluid Science

journal homepage: www.elsevier.com/locate/etfs

Experimental analysis of flow topology and particle behavior in microcavities

Paulius Vilkinis *, Justas Šereika, Gediminas Skarbalius, Algis Džiugys, Nerijus Pedišius

Laboratory of Heat-Equipment Research and Testing, Lithuanian Energy Institute, Breslaujos str. 3 Kaunas, LT-44403, Lithuania

A B S T R A C T

Efficient hydrodynamic particle trapping requires the precise control of flow structures that serve as hydrodynamic traps. Microfluidic structures, such as microcavities of various shapes and sizes, can be applied as hydrodynamic traps, and the exerting force can be controlled by changing the geometrical parameters and flow regimes of the cavities. In this study, the capability of trapping microparticles in rectangular, semicircular, and triangular microcavities is experimentally investigated. The flow structure in microcavities with a length-to-depth ratio L/h of 1–4 for rectangular cavities and L/h = 1–2 for semicircular and triangular cavities at a Reynolds number ranging between 1 and 1000 is visualized using a microparticle image velocimetry system. Additionally, patches of 20 μm particles are visualized using a high-speed camera. Different flow phases, namely attached, transitional, and separated, are observed and correlated with the cavity parameters and flow regime. Additionally, qualitative flow parameters determining particle behavior, such as the vortex center location and temporal vortical stability, are analyzed. Finally, the particle behavior is correlated with the flow structure in the cavities, and guidelines for the development of the optimal design of micro- and nanofluidic devices are discussed.

1. Introduction

Precise control of microscale fluid flow is critical in biotechnological applications. Microfluidic structures such as microcavities have been widely applied in biomedical, biochemical, and high-throughput screening applications [1,2]. In particular, particle trapping, docking, alignment, sorting, and the size-based separation of cells and particles have been widely investigated [3]. Inertial microfluidics can be used to address the diverse problems in flow control for various biomedical applications. Particles or cells in flowing microfluidic devices are exposed to hydrodynamic forces such as wall, shear, and centrifugal forces [4–6]. The inertial forces can be controlled by varying the flow and geometrical parameters. Passive flow control can be easily achieved by exploiting the dependence of hydrodynamic forces on microchannel geometry.

Recently, researchers have directed their flow-structure research toward microfluidic applications. The shapes of the microfluidic geometries, volume flow rates, and flow structure results were selected and analyzed based on the microfluidic applications. In recent years, the increased use of microcavities has been observed in cell trapping [7–9], docking [2,10], and separation [6,11,12] applications. The flow phenomena must be examined comprehensively in advance to select the required geometry and flow conditions to achieve the desired effects. Many experimental and numerical studies on vortex structure and dynamics in rectangular and square cavities serve as a benchmark for many fluid mechanics problems. Flow morphology has been investigated extensively. Faure et al. [13] experimentally investigated the effect of cavity aspect ratio on vortical structures at medium-range values of the Reynolds number (Re). Cheng and Hung [14] numerically analyzed the vortex structure based on a wider aspect ratio (0.1–7) and Re range. They concluded that the number of vortices and their structure depended on both the aspect ratio and Re. Sheryl et al. [15] demonstrated that in a shallow rectangular cavity, a single vortex was generated downstream of the cavity in laminar and turbulent flow regimes, and that the vortex strength depended on the upstream boundary layer. Yu et al. [16] investigated rectangular cavities with varying aspect and span ratios. The authors showed that rectangular cavities varying in dimensions, location, and number of cavities barely affected the flow in the microchannels; the only effect observed was an increase in the mass flow rate with the number of cavities. The flow pattern in the cavity was governed by the Re, span ratio, and cavity aspect ratio. The critical values of Re and the span ratios indicate whether the flow in the cavity is attached or separated. Typically, regular-shaped cavities are investigated (right angles). However, a recent study [17] showed that rounded cavity corners reduced the recirculation zone length and pressure losses in the cavity, while increasing flow instability.

* Corresponding author.
E-mail addresses: paulius.vilkinis@lei.lt (P. Vilkinis), justas.sereika@lei.lt (J. Šereika), gediminas.skarbalius@lei.lt (G. Skarbalius), algis.dziugys@lei.lt (A. Džiugys), nerijus.pedisius@lei.lt (N. Pedišius).

https://doi.org/10.1016/j.expthermflusci.2023.111046
Received 7 April 2023; Received in revised form 4 August 2023; Accepted 29 August 2023
Available online 31 August 2023

Flows in square or rectangular cavities are primarily investigated in most studies; however, non-rectangular cavities are desirable or may exhibit better properties for certain applications in some scenarios. Fishler et al. [18] investigated the evolution of vortices (number, location, center, and existence of saddle points) in cylindrical cavities based on the flow regime and geometrical parameters of the cavities. The authors provided phase diagrams that facilitated the selection of a cavity that can achieve the desired recirculating flow structure. In addition, the rotation frequencies in cavities featuring single vortices were provided. Ozalp et al. [19] investigated flow statistics and the effect of cavity shape on the flow structure in rectangular, triangular, and semicircular cavities, and then analyzed the effect of the shape and Re on the turbulent quantities in each cavity. Mercan and Atalik [20] investigated the flow structure in arc-shaped cavities with different aspect ratios and identified the number of secondary vortices based on the aspect ratio at high Re.

Regarding the behavior of particles in microcavities, Jiang et al. [9] numerically investigated the dynamics of a single particle in a micro-vortical flow inside a microcavity. Based on the Re, three particle-entrapping phases (no trapping, stable, and unstable trapping) and four particle-trapping modes (outer to inner, invariable, inner to outer, and inner to escape) were observed. The trapping of particles depends on Re and the Stokes number. Dhar et al. [8] showed that the entry channel dimensions affect the entrapment efficiency. Smaller channel cross-sections and sharper parabolic velocity profiles increased the shear-gradient lift force, which directs particles to the cavity. Zhou et al. [6] showed that additional vortices in parallel vertical planes were formed at high Re, which resulted in particle trapping. In addition, the critical Re value at which the particles were entrapped in the cavity depended on the cavity length and particle diameter. Shen et al. [21] and Lim et al. [22] experimentally demonstrated that the particle size, density, and Re affected the path of particles in a vortex. By altering drag and shear forces, Basagaoglu et al. [23] showed that smooth shapes of cavities and obstacles affected the particle-trapping efficiency.

Although the flow structure in cavities and particle behavior in flows have been investigated extensively, more research is necessitated to correlate the characteristics of controlled flow in cavities with particle behavior and trapping efficiency. In this study, the flow structures in rectangular, semicircular, and triangular cavities with rounded bottom corners are analyzed experimentally based on the flow regime in a wide Re range and relative cavity length. Furthermore, the particle behavior under each Re and length-to-depth ratio (L/h_1) is investigated using 20 μm diameter microparticles. This behavior is shown to be associated with the flow structure, vortex center location, and temporal variation in the vortices. In this work, particle trapping dynamics were compared in rectangular, semicircular, and triangular cavities with rounded corners. To the authors' knowledge the qualitative analysis of flow structure and its relation to particle trapping is performed for the first time. This study extends the research area of flow dynamics in microcavities, where shear layer growth is caused by the interaction of separated and recirculated flows. The results may facilitate the development of the optimal design of micro- and nanofluidic devices.

2. Experimental setup and methods

Experiments were conducted in microchannels with rectangular, semicircular, and triangular cavities of different sizes (Fig. 1). The channel had a rectangular cross-section (width: 0.9; height: 0.3 mm).

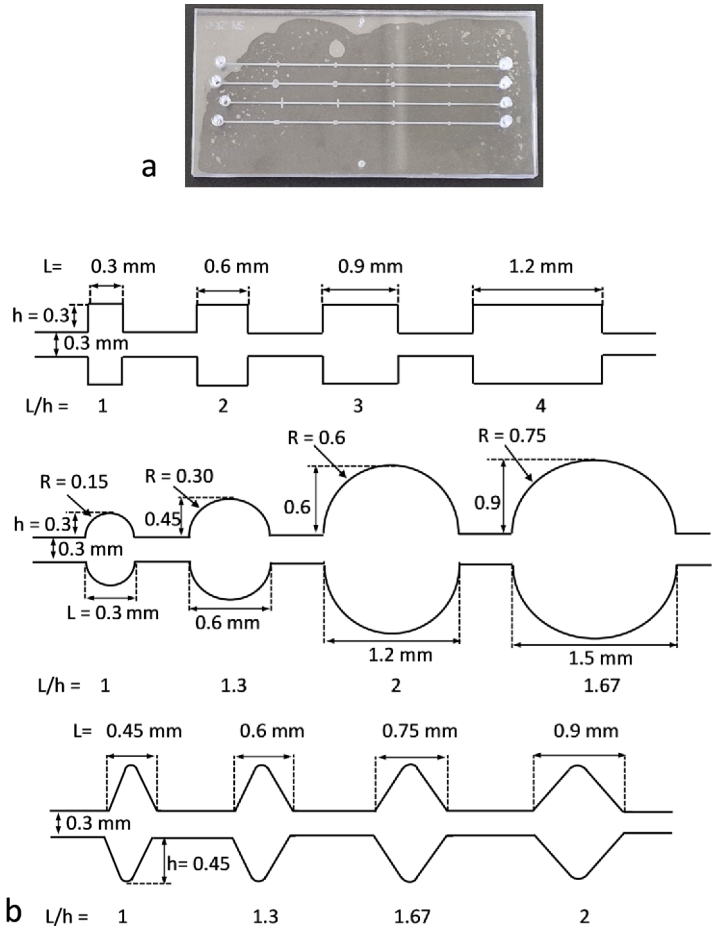

Fig. 1. A) Image of microchannel chip. Note: deep cavities (third channel from the top) are not used in this research; b) geometry of used microchannels with microcavities.

Microchannels are manufactured in acrylic glass plates using high accuracy micro milling technology. Channels with cavities are cut in one acrylic plate and then covered and sealed with another plate. Each channel is 80 mm in length including inlet and outlet ports. These ports are 1.2 mm diameter and cut-off needles are used to connect the hose. The distance between cavities is 15 mm, which exceeds ten channel widths and ensures that the flow is fully developed before each cavity. Cavities are con in both sides of the channel. The length of the rectangular and triangular cavities increased, whereas their depth remained constant. Meanwhile, the length, depth, and curvature R of the semicircular cavities increased. Thus, the relative cavity length L/h values of the rectangular cavities were 1, 2, 3, and 4. For the semicircular and triangular cavities, the relative length L/h values were 1, 1.3, 1.6, and 2. The rectangular and triangular microcavities exhibited rounded corners, which was due to the manufacturing process involved.

A microparticle image velocimetry (μPIV) system was used for quantitative flow visualization inside the microcavities. Nile Red fluorescent particles (excitation 535 nm, fluorescent 575 nm, and mean diameter 1.1 μ; Invitrogen) dispersed in deionized water were used for flow visualization, and 1 % v/v Tween 20 surfactant was used to reduce the possibility of particle adhesion to the walls. The fluid temperature was maintained at 21 + 2 °C. The fluid flow was controlled using an ElveFlow OB1-MK3 pressure controller with an external pressure source. The μPIV system used comprised Nd:YAG dual-cavity laser (DantecDynamics), an LPU 450 laser control unit (DantecDynamics), and a FlowSense EO CCD camera (DantecDynamics) coupled with a Leica DM ILMD microscope (Leica Microsystems). The system was operated at a frequency of 15 Hz. The DynamicStudio (DantecDynamics) software was employed for the system control of image acquisition and post-processing. The time between image pairs varied from 1 to 1500 μs depending on the flow rate. The time-averaged velocity data were obtained by averaging at least 200 images. An adaptive correlation algorithm was applied for image processing. The vector spacing of the processed image data was 2.5 and 1.5 μm in the streamwise and spanwise directions, respectively.

Polystyrene microparticles measuring 20 μm (Merck Group) were used for particle tracking experiments. The relative density of the particles was 1.05. Particle images were captured using a Ximea CB019MG camera operating up to 2263 FPS at a resolution of 2 Mpix and higher FPS at reduced resolution. During the measurements the resolution was reduced to achieve a sufficient sampling rate for the accurate tracking. For particle tracking the ImageJ software with MTrackJ plugin is employed. To highlight particles in the flow, the raw images are processed by subtracting the median of whole ensemble form each single image. Later, bandpass and threshold filters are applied to remove noise and enhance particle images. Particles tracking is performed by taking the coordinates of single particle at each image. For representation particle coordinates are exported and depicted on a schematic cavity drawing. In Fig. 2 raw and processed images with particle tracks are presented.

Flow condition is characterized by Reynolds number based on hydraulic diameter of the microchannel $Re = \frac{QD_h}{A\nu}$, where Q, D_h, A and ν are volumetric flow rate, hydraulic diameter, channel's cross-sectional area and kinematic viscosity, respectively. Measurements are performed at Re range 1–1000 corresponding to flow rate of 5.8×10^{-10} –5.7×10^{-7} m^3/s and mean velocity 2×10^{-3} – 2 m/s.

Stokes number is defined as $= \frac{\rho_p d_p^2 \nu}{18} \mu D_h$, where ρ_p, d_p, and μ are particle density, particle diameter and fluid dynamic viscosity respectively. For 20 μm diameter microparticles Stk is 1.1×10^{-5} – 1.1×10^{-2} for investigated Re range. As Stk ≪ 1, particles are following flow streamlines carefully.

3. Results and discussions

3.1. Vortex structure in cavities

The characteristic flow fields of the attached, transitional, and separated flow regimes [24] are shown in Fig. 3. This flow structure differentiation is based on recirculation zone and separated shear layer structure and behavior in the cavity, and is widely used in similar research [18,24,25]. Two-dimensional velocity vector maps were obtained for the middle plane of the cavity. Additionally, velocity distributions for three flow patterns at Re = 1, 100 and 1000 are presented in Fig. 4. Velocity profiles are measured at vertical and horizontal planes along the vortex center. In the cases of attached flow, velocity profiles are measured along the cavity center. In vertical and horizontal planes u_x and u_y velocity components are measured, respectively. Velocities are normalized by the average velocity in the main channel U. The flow evolution and changes in the vortex topology depended on the Re and cavity geometry. A cavity aspect ratio of L/h = 2 was selected to compare the flow topologies in cavities with different geometries.

At a low Re (Re = 1), the flow passed through the cavities without separation. As no circulation is observed in the cavity flow regime is defined as attached. In this flow regime horizontal velocity component u_x decays rapidly along the cavity. In the case of rectangular cavity, the decay is almost linear, while in semicircular and triangular cases decay rate is higher in the center part of cavity determined by smaller streamlines curvature. The vertical velocity component u_y features saddle point in the center part of cavity (x/L = 0.5–0.6). As the Re increased slightly (Re = 10), a small vortex formed in the corner near the leading wall of the cavity. In a rectangular cavity, the vortex occupied only a small upstream region of the cavity and exhibited both separate and attached flows, whereas in a semicircular cavity, the vortex was elongated along the bottom of the cavity and reached the trailing wall. In the triangular cavity vortex occupied the entire lower region of the cavity. As the cavity volume decreased, the velocity decayed, and the pressure and adverse pressure gradient in the cavity increased; therefore, a stronger vortex was formed in the lower-volume cavities. Because vortices occupied only a small region of the cavities, the shear layer was thick, and minimal energy was transferred from the main flow to the flow in the cavity; thus, the velocity in the cavity was relatively low compared with that in the main flow. Since the flow structure is characterized by attached and separated flows and formed vortex is weak and occupies only a fraction of cavity volume, flow regime is defined as

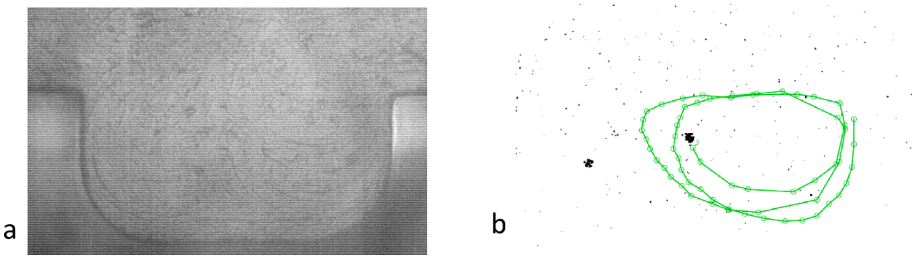

Fig. 2. A) Unprocessed image of flow in rectangular L/h = 2 cavity, where particles are barely seen and b) processed image of flow where particles' images are enhanced and a track of single particle.

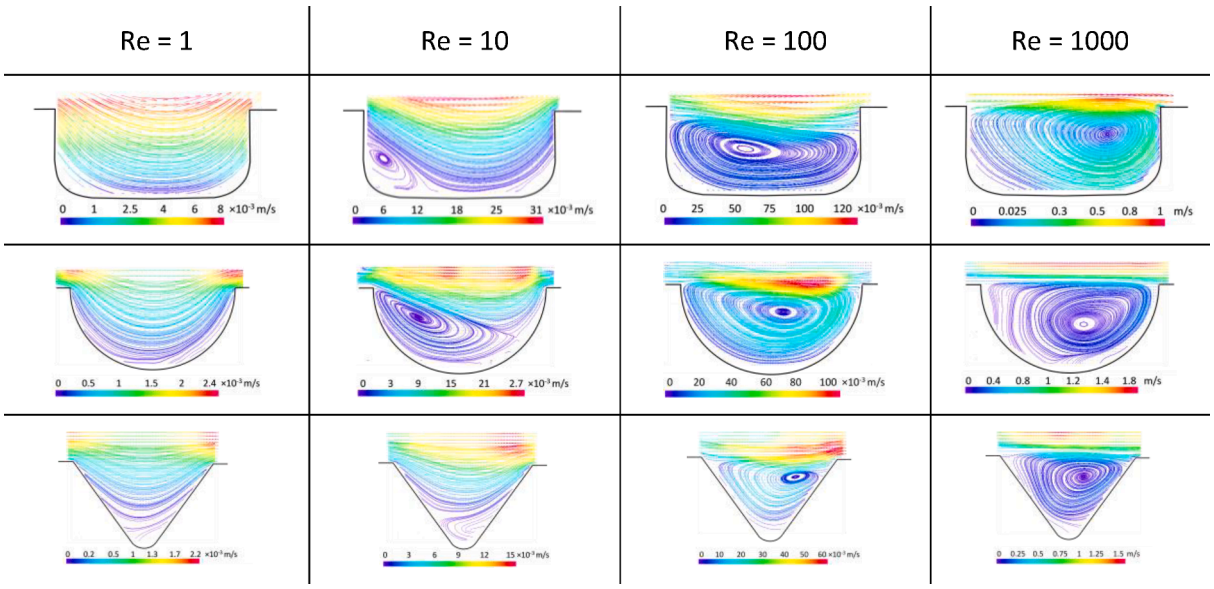

Fig. 3. Streamlines of attached, transitional, and separated flows in each type of cavity (L/h = 2).

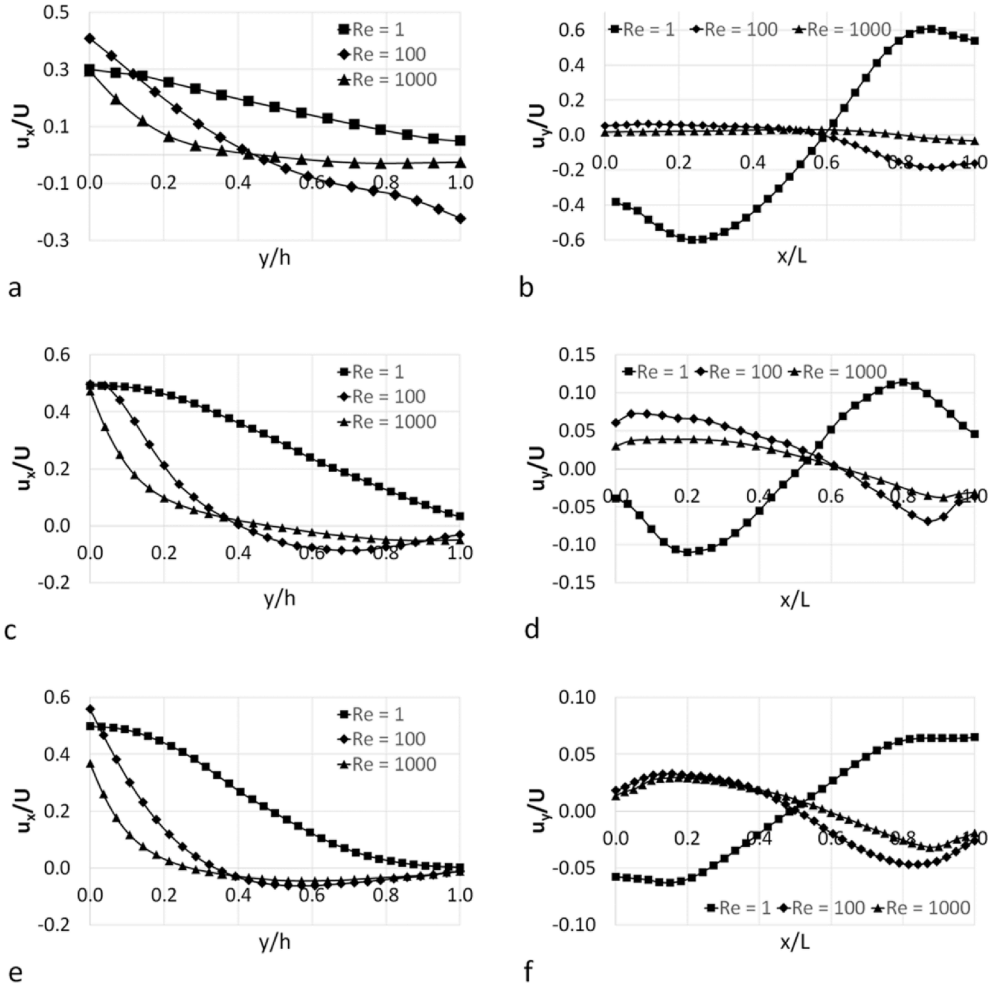

Fig. 4. Vertical and horizontal velocity profiles in a) and b) rectangular, c) and d) semicircular, and e) and f) triangular cavities.

transitional. As the Re increased further up to Re = 100, the vortices expanded; however, the growth was confined by the trailing wall of the cavity. At Re = 1000, the vortices occupied most of the cavities and the main flow was ejected from the cavity. In this flow regime, the vortex topology reached its final form in the semicircular and triangular cavities. However, in a rectangular cavity, the position the vortex center

shifted from the leading to the trailing wall of the cavity as Re further increased. In the semicircular and triangular cavities, the vortex center shifted slightly downstream as the vortex intensity increased. At a high Re, the shear layer became thinner and more energy from the main flow was transferred to the cavity flow; thus, the velocity in the cavity increased. As flow is characterized by mostly the recirculating flow in the cavity and does no longer depend on Re, the flow structure is defined as separated. Horizontal and vertical velocity profiles appear similar at Re = 100 and 1000. Horizontal velocity decreases along the cavity and reaches $u_x/U = 0$ at $x/L \approx 0.4$ and then becomes negative. At Re = 100, slightly higher negative values are reached because vortex center is located in the middle part of cavity and backward flow is still able to accelerate, while at Re = 1000, the backward velocity remains almost constant. Although velocity profiles are similar at Re = 100 and 1000, differences in flow stability remain, which will be further analyzed in Figs. 7-14.

The similar flow structure results, although in slightly different geometry cavities, are presented by Shen et al. [21,24], Jiang et al. [9], and Liu et al. [26] in rectangular cavities, Fishler et. al [18] in circular cavities, and Ozalp et al. [19] in rectangular, semicircular and triangular cavities.

Design guidelines showing the flow topology in cavities based on geometrical and flow parameters may facilitate the design of application-driven microcavities. To establish the critical conditions for the transition of the flow configuration in the cavity, three flow patterns were mapped as functions of Re and L/h (Fig. 5).

Based on the phase diagrams, the flow in the cavity may be attached if either Re or L/h is low. However, rectangular and semicircular cavities feature separated flow at low Re and L/h $\leq$ 1, where a single vortex structure appears on the bottom of the cavity. In the triangular cavity, the flow is attached at all investigated L/h at Re $\leq$ 10. This is associated with a more gradual channel expansion compared with the result yielded by the other two types of cavities, which alleviates velocity decay and adverse pressure gradients, thus delaying vortex formation. As L/h increased, the effect of the trailing wall diminished, and the flow in the cavity was dominated by the main flow. Transitional flow occurred at Re > 10 in the semicircular and triangular cavities, and at Re $\geq$ 20 (until Re = 100) in the rectangular cavities, depending on the cavity type and L/h. The transitional flow featured both recirculation and attached flows in the cavity. As Re increased, the vortex expanded; consequently, it became confined by the trailing wall of the cavity and ejected the main flow from the cavity. The transitional flow was the longest in the rectangular cavity because as the cavity length increased, a greater main flow was required to maintain the recirculation zone.

The cavity size affects the flow regime in the cavity. A comparison between our results and those of other studies revealed some differences. In this study, in the rectangular and semicircular cavities, the flow was separated at low Re and L/h values. However, in the studies by Shen et al. [24] and Yu et al. [16] for rectangular cavities and Fishler et al. [18] for circular cavities, the flow remained attached at low Re. In these studies, either the cavities or channel sizes were relatively small (<100 μm) and the channels exhibited a high aspect ratio, which reduced the three-dimensionality of the flow in the cavities, thus allowing for an attached flow regime at low Re.

3.2. Temporal vortical evolution

As shown in Fig. 6, the vortex center changes its location based on the Re and cavity geometry. The vortex center location was measured in the X- and Y-directions; here, x/L = 0 and x/L = 1 correspond to the leading and trailing walls of the cavity, respectively. Similarly, y/h = 0 and y/h = 1 correspond to the bottom and lid of the cavity, respectively. Cavity lid is considered to be at the boundary between channel and the cavity. In general, the location of the vortex center shifted significantly at low Re (Re ⟨200) and became more stable as Re increased. The stable position in the rectangular cavity was attained at a

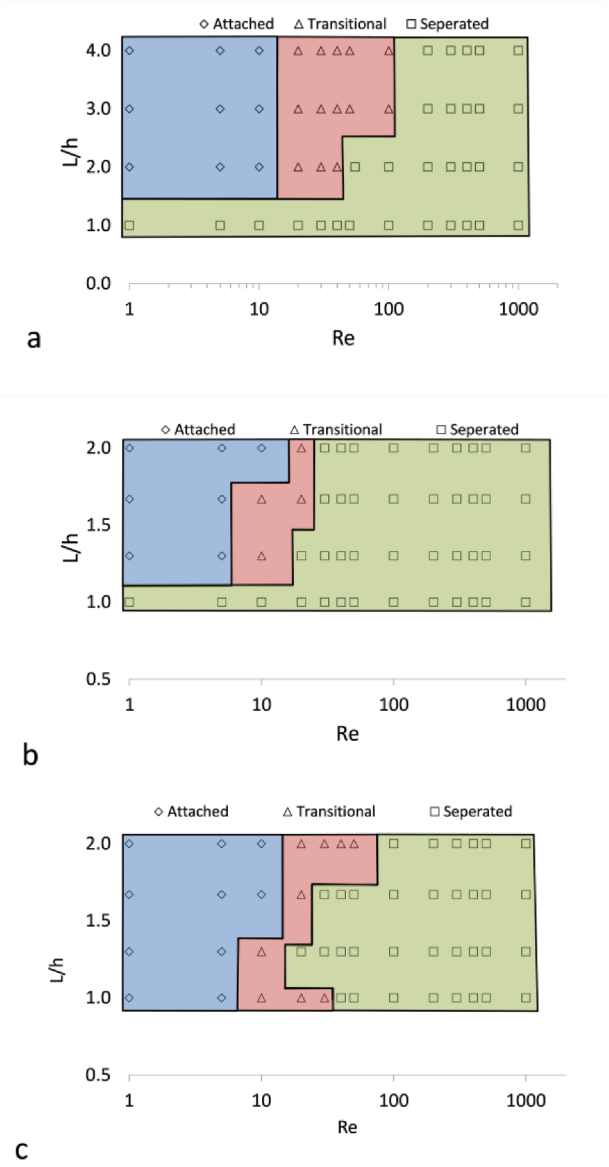

Fig. 5. Phase diagrams of cavity flow regimes in a) rectangular, b) semicircular, and c) triangular cavities.

higher Re compared with the case for the semicircular and triangular cavities because, owing to the higher cavity volume, a higher velocity was required for the vortex to reach its stable form.

At a low Re, a small vortex was formed behind the leading cavity wall or on the bottom of the cavity, which expanded as Re increased; simultaneously, the vortex center shifted downstream in the X-direction and toward the cavity lid in the Y-direction. At Re > 200, a slightly opposite shift was observed in the semicircular and triangular cavities. As the vortex became bulkier, it propagated upstream and toward the cavity bottom to fit into the cavity. In the rectangular cavity, the vortex center position was stable because of the larger cavity volume, which allowed the vortex to expand without changing its location.

To better understand the dependence of the flow structure on the cavity geometry, the instantaneous flow fields are presented in the following figures. The four consecutive time instances with time interval of 0.067 s and whole sample averaged flow fields are presented in the following figures. The total time interval between T1 and T4 is ~ 0.017 s. The flow fields are presented at three different L/h values and Re corresponding to the attached, transitional, and separated flow modes. In certain cases, the cyclicity of flow structure is observed.

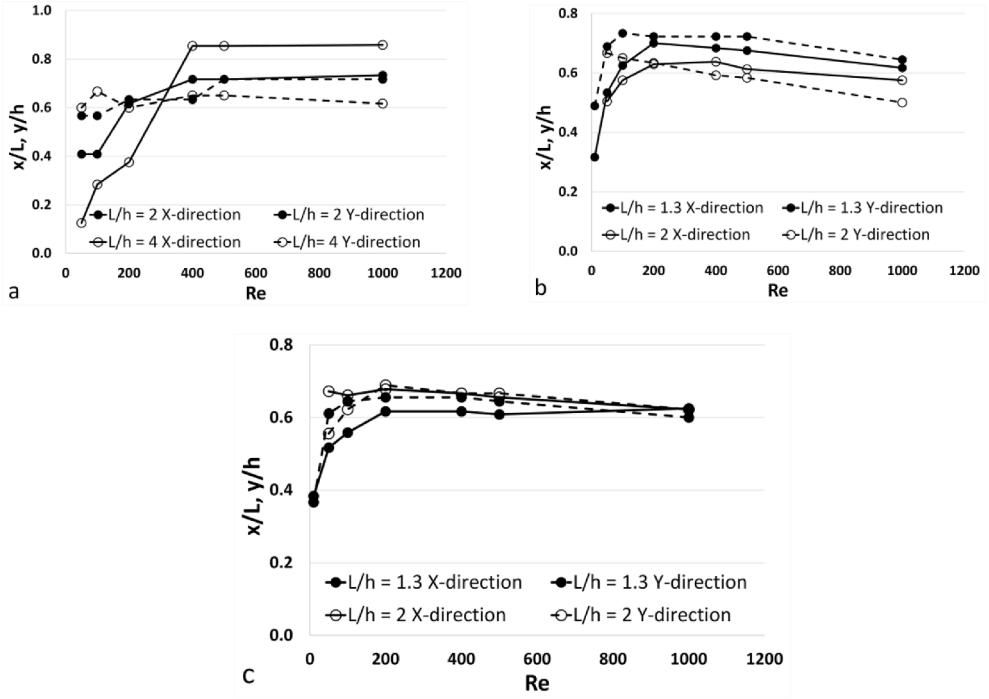

Fig. 6. Vortex center location dynamics in a) rectangular, b) semicircular, and c) triangular cavities.

In Figs. 7–8, the instantaneous flow fields for relative rectangular cavity lengths L/h = 1, 2, and 4 are presented. In the case of a short cavity (Fig. 7), a single vortex was observed at every instance. The flow topology in the cavity was stable throughout the investigated Re range. Only a slight cavity center shift toward the trailing wall was observed at certain time instances. As the relative cavity length increased (Figs. 7 and 8), the pressure gradient became overly weak, which hindered the generation of a permanent vortex in the cavity at Re = 10. A small vortex was observed behind the leading cavity wall at certain instances. The vortex was present for approximately one-half the observed time interval. At a higher Re (Re = 100) cyclicity of flow structure in L/h = 2 is observed. At the initial time instance, the cavity was filled with an elongated vortex whose center was located near the leading cavity wall. Over time, the position of the vortex center shifted, and the vortex propagated along the cavity. As the vortex center reached the middle region of the cavity, the vortex was segregated into two. At a later instance, the second vortex located behind the trailing wall was ejected from the cavity and the cycle restarted. In this flow regime, the flow velocity in the cavity was relatively low compared with the velocity of the main flow. In addition, the main flow occupied the upper region of the cavity, thus resulting in high shear stresses in the interaction between the cavity and main channel flows. As Re increased further (Re > 100), the main flow was completely ejected from the cavity and the recirculation flow intensified. The vortex center was fixed behind the trailing wall of the cavity at each time instance. At this flow rate, the velocities of the recirculation flow became comparable to those of the main flow; thus, the shear stress at the intersection reduced, and the flow topology in the cavity stabilized. As the cavity length increased further (L/h = 4), no small short-lived vortices were observed behind the leading cavity wall at Re = 10. At Re = 100, the vortex length changed slightly over the time. A stagnation point was observed at the end of the vortex and at the high-curvature streamlines behind the trailing cavity wall; however, no secondary vortex formation was observed. At Re = 1000, the vortex center was located behind the trailing cavity wall. In this case the cyclicity is observed analogous to L/h = 2 at Re = 100 case. The secondary vortex, which formed as a boundary layer attached to the

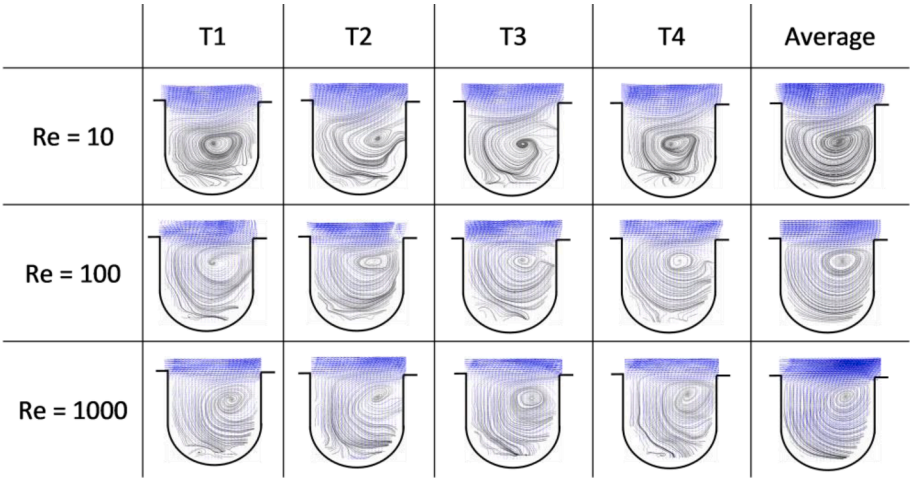

Fig. 7. Instantaneous and averaged streamlines in rectangular cavity at L/h = 1 and different Re.

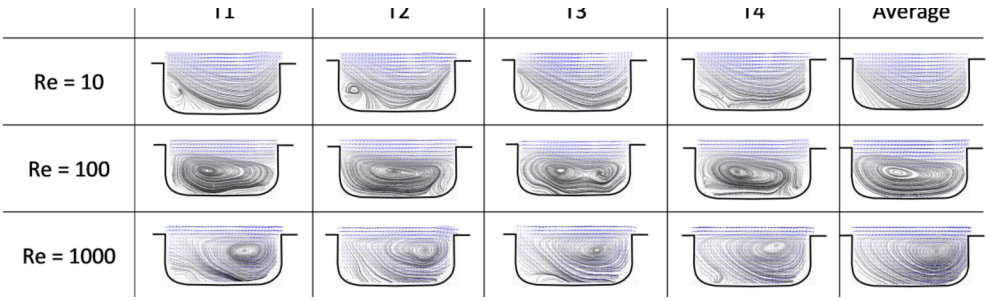

Fig. 8. Instantaneous and averaged streamlines in rectangular cavity at L/h = 2 and different Re.

leading edge of the cavity [27], appeared in the front region of the cavity and dissipated rapidly with the main vortex.

In Figs. 10 and 11, the instantaneous flow fields in semicircular cavities with L/h = 1.6, and 2 are presented. The case of L/h = 1 is not presented as it is identical to rectangular cavity at the same length-to-depth ratio. The flow fields in the case of L/h = 1 were similar to those in the rectangular cavity under the same L/h because the bottom of the rectangular cavity was slightly rounded, i.e., the geometries of both cavities were the same. At L/h = 1.6, the vortex expanded as Re increased; however, the vortex structure remained stable over the time. At L/h = 2 and Re = 10, the vortex behind the leading wall of the cavity was observed only in certain time instances, and no vortex was observed in the average flow field. Thus, the flow was fully attached to the cavity. As Re increased, the vortex occupied the entire cavity, and the location of the vortex center changed only slightly during the cycle. At Re = 1000, the vortex propagated to the trailing cavity wall and high-curvature streamlines were observed near the leading cavity wall. The flow structure became more chaotic as the cavity length increased. Small vortices were generated behind the leading cavity wall and dissipated abruptly along with the main vortex. These vortices could not be captured during the experiment because of their short lifetimes. Similar phenomena were observed in the rectangular cavities. Hence, one may conclude that the turbulence in the recirculation zone increases with the cavity length.

For the triangular cavity (Figs. 12–14), a vortex was observed at the bottom of the cavity at certain time instances at Re = 10. However, as L/h increased, the vortex intensity in the cavity decreased. Therefore, in the average flow field, a vortex was observed in the cases of L/h = 1 and 1.6, whereas only curved streamlines were shown at L/h = 2. In general, when L/h = 1, the flow topology in the cavity was similar to that in short rectangular and semicircular cavities. As Re increased, the vortex occupied the entire cavity. The vortex structure remained stable over the time at Re = 100 and 1000, and only a slight vortex center movement was observed. The recirculation zone in the triangular cavities was the most stable of all investigated Re values compared with the case of the rectangular and semicircular cavities. Vortex movements in the cavity were restricted by the sidewalls, and the space for the generation of short-lived eddies behind the leading cavity edge was insufficient; therefore, the effect of cavity instability decreased significantly.

3.3. Particle tracking in cavities

In the following figures (Figs. 15, 16 and 17), particle tracking in rectangular, semicircular, and triangular cavities with different L/h values is depicted at Re values of 10, 100, and 1000. The particle is considered trapped in the cavity if it circulates in the stable orbit for a sufficient long time. In this case the particle images were recorded for 2–3 s. If the particle was found circulating in the stable orbit, we consider it as trapped. If particle leaves the cavity after single or several rotations the trapping is considered unstable. The entrapment of particles in the recirculation zone depends on the flow regime and cavity length. In all cases it is observed that initial particle position influences trapping efficiency. Only the particles located closest to the side wall could be drawn into the cavity. The shear lifting force acting on the particle is sufficient to direct particles into the cavity only if particles are moving close to the cavity opening. In the case of a short rectangular cavity (L/h = 1) (Fig. 15), the particles passed through the cavity at Re = 10 and 100 because the shear lifting force exerting on the particle was insufficient for the particle to be drawn into the cavity. As Re increased to 1000, the particles were entrained into the recirculation zone, showing a stable circulation patch. Obtained particle patches are comparable to ones presented by Jiang et. al [9] and Shen et al. [21,28] in rectangular cavities. Arguably, in our case the stable trapping is reached at higher Re due to differences in geometrical parameters and three-dimensional flow caused by a high channel aspect ratio. For longer cavities (L/h = 2 and 4), the particles passed through the cavities at Re = 10. As Re increased further, the particles were entrapped in the L/h = 2 cavity. At Re = 100, the particle path was stable for several rotations, with a clear exit path. At Re = 1000, the particle remained entrapped, and its path was shifted from the inner to the outer orbit. As the cavity length further increased to L/h = 4 at Re = 100, the particles entered the cavity at the leading edge and precisely followed the streamlines. After a single rotation along the cavity and vortices behind the leading and trailing edges, the particles departed from the cavity at the trailing edge.

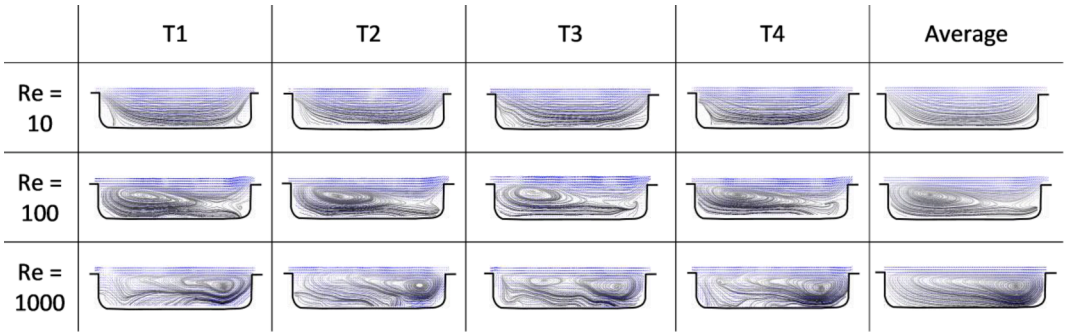

Fig. 9. Instantaneous and averaged streamlines in rectangular cavity at L/h = 4 and different Re.

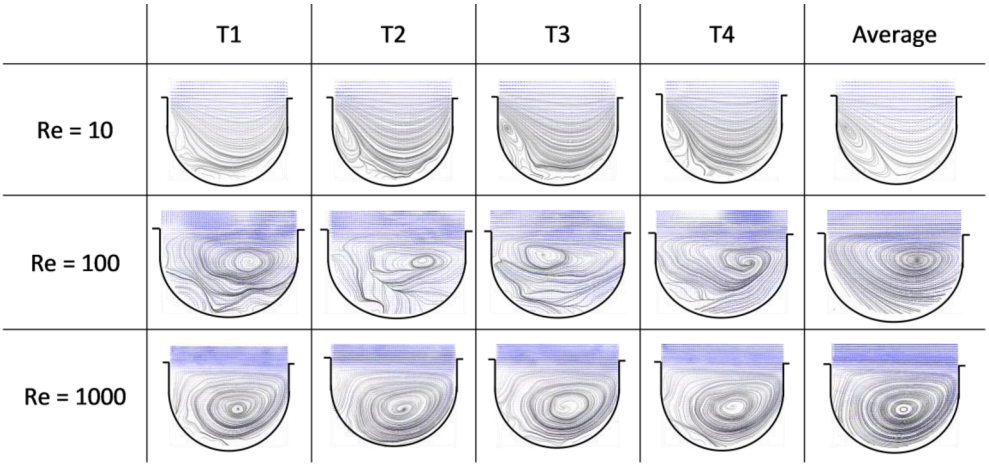

Fig. 10. Instantaneous and averaged streamlines in semicircular cavity at L/h = 1.6 and different Re.

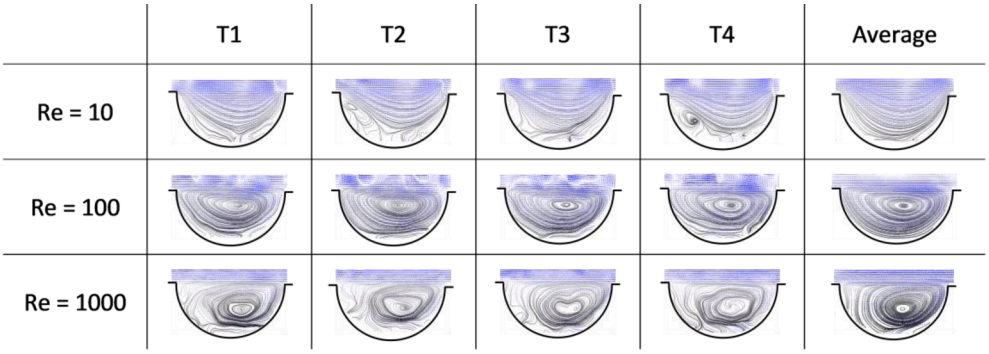

Fig. 11. Instantaneous and averaged streamlines in semicircular cavity at L/h = 2 and different Re.

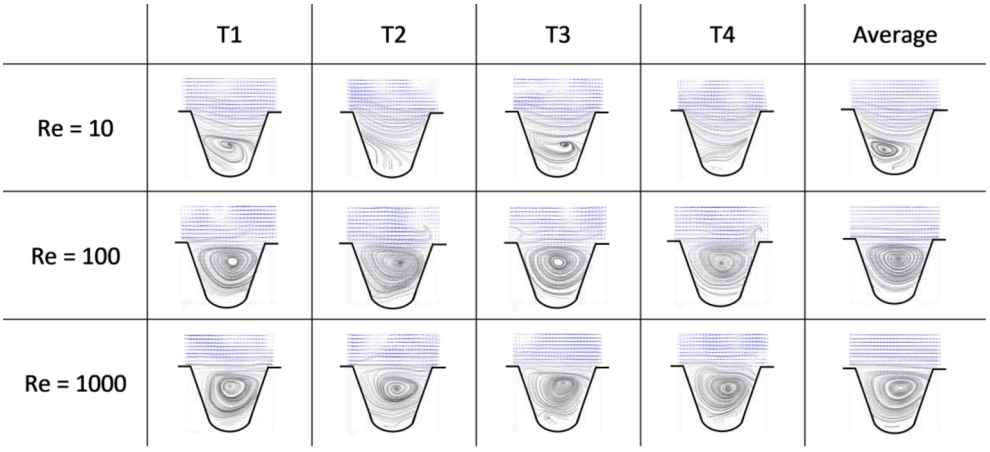

Fig. 12. Instantaneous and averaged streamlines in triangular cavity at L/h = 1 and different Re.

At Re = 1000, a particle was entrapped at the trailing edge, and its path changed from the inner to the outer orbit. Subsequently, the particle migrated to the parallel plane, where it could no longer be tracked. No exit path from the cavity was observed, indicating that either the entrapped particles remained trapped in the cavity or left the cavity at planes closer to the sidewalls. This particle behavior indicates that flow in cavities is three-dimensional. Either narrower channel or bigger particles should be used to reduce this effect.

For the semicircular cavities (Fig. 16), the case of L/h = 1 is not shown owing to the rounded cavity bottom, which implies that the geometry and flow fields are identical to those of the rectangular L/h = 1 case. As the cavity length increased to L/h = 1.6 and 2, the particles in both cavities exhibited similar behaviors. At Re = 10, the particles were entrained into a small vortex behind the leading cavity wall, whereas most of the particles passed above the cavity. Subsequently, the entrapped particles migrated from the inner to the outer orbit. As the outermost orbit merged with the particle patch above the cavity, the particles escaped the vortex. At a higher Re, the particles entered the cavity at the trailing edge. The particles experienced a high inertial centrifugal force at a high Re and were entrapped in the outer orbit. As the velocity decreases inside the vortex, the particles can switch patches to the inner orbit. After several rotations, the particles disappeared from

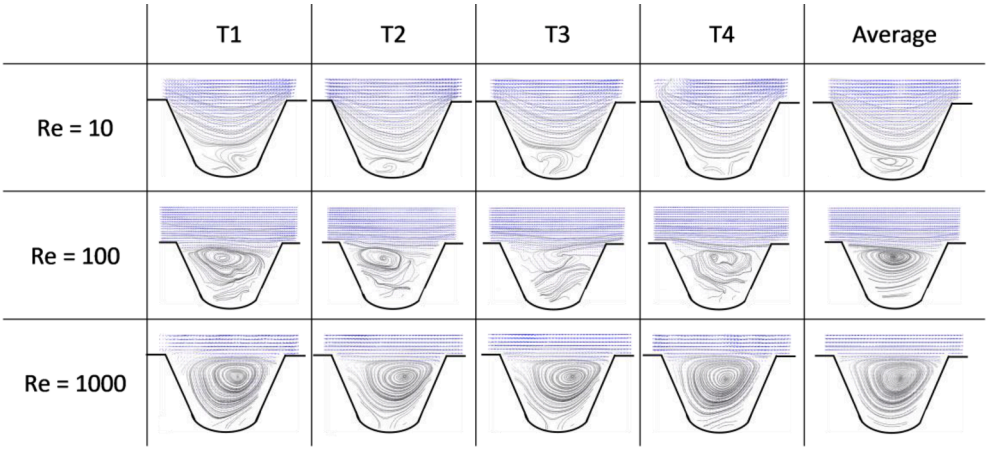

Fig. 13. Instantaneous and averaged streamlines in triangular cavity at L/h = 1.6 and different Re.

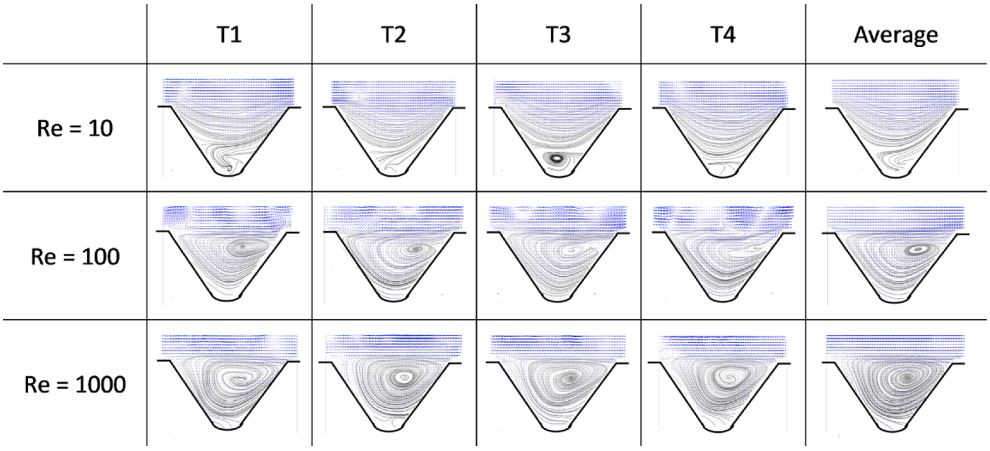

Fig. 14. Instantaneous and averaged streamlines in triangular cavity at L/h = 2 and different Re.

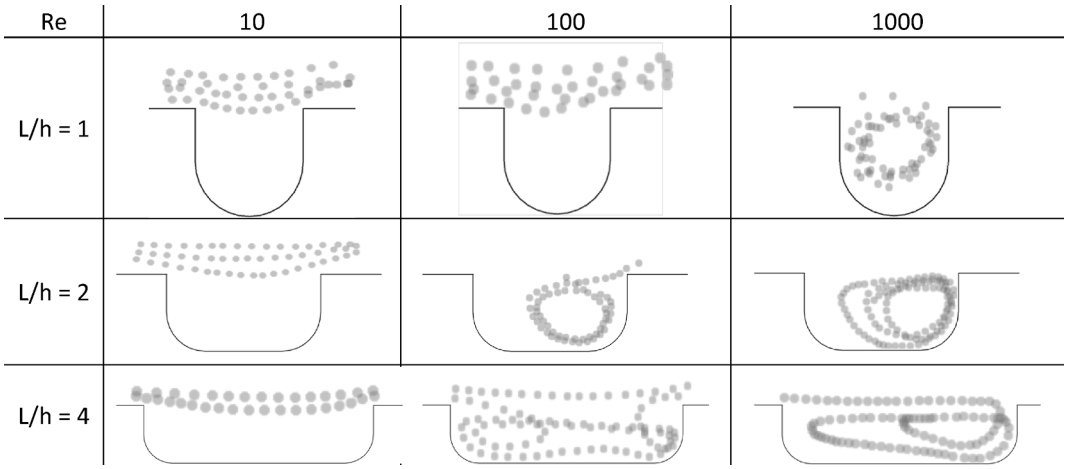

Fig. 15. Particle trajectory in rectangular cavities.

the vertical plane, indicating the formation of additional vortices across the cavity depth. At L/h = 1.6, the change in the vertical plane occurred more abruptly than that at L/h = 2, where the particles remained in the investigated vertical plane for a longer period.

In the case of the triangular cavities (Fig. 17), the particles passed above the cavity at Re = 10 and 100 in all investigated cases. However, at Re = 1000, regardless of the L/h ratio, the particles were entrapped in a single orbit. The most stable orbit was observed at L/h = 1. A stable orbit is a consequence of the selective entrapment of the particles. Some particles passed above the cavity, indicating that only a few particles were entrapped, thus resulting in a stable orbit. When L/h increased, the particle path became distorted, indicating the formation of an additional orbit. However, the particles remained trapped in the cavity throughout the measurement period.

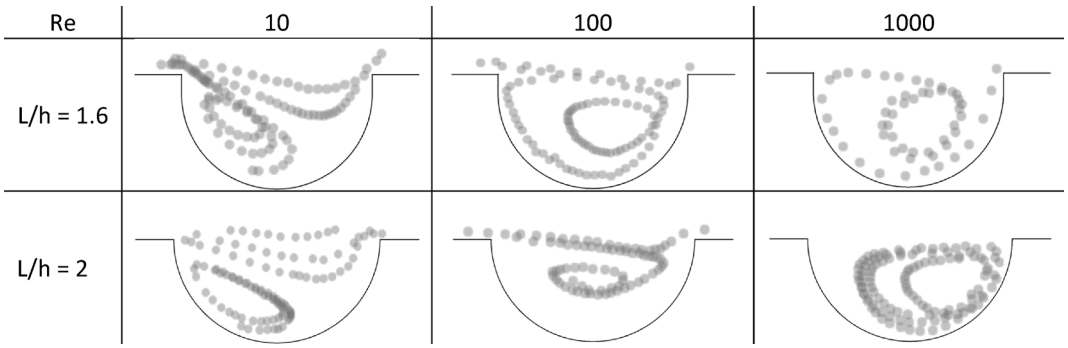

Fig. 16. Particle trajectory in semicircular cavities.

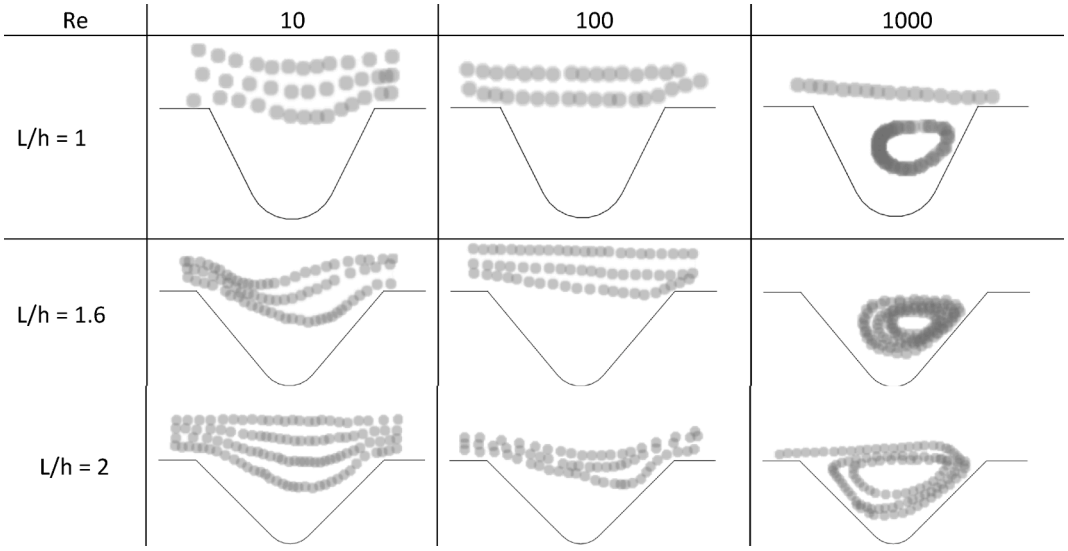

Fig. 17. Particle trajectory in triangular cavities.

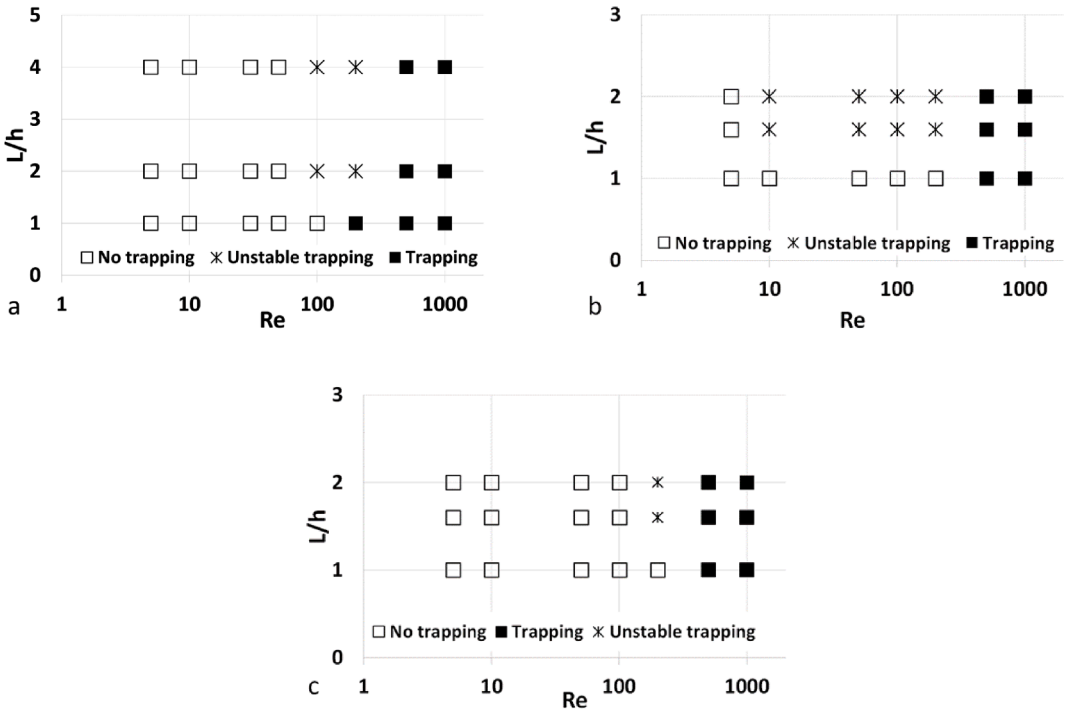

Fig. 18. Particle behavior modes in a) rectangular, b) semicircular, and c) triangular cavities.

3.4. Relationship between flow structure and particle behavior

The flow topology is vital to particle trapping in cavities. Jiang et al. [9] showed that a flow must be separated for particle trapping. Particles cannot be trapped in an attached flow, and trapping is unstable in a transitional flow [24]. The particle trapping results are summarized in Fig. 18. As shown, the particle trapping modes are consistent with the flow phase diagrams presented in Fig. 3. In most cases, vortices were present in the cavities at Re $<$ 100. However, these vortices were generally weak, and the inertial lift force was insufficient for the particles to migrate through the thick shear layer. In the case of semicircular cavities, a few particles were entrained into the cavity because of the specific vortex shape, which mitigated the boundary between the separated shear layer and recirculating flow. Nevertheless, the particles remained trapped for a short time because of the unstable vortex structure. In all the other cases, the particles passed above the cavity in the same manner as if no vortex was present.

As Re increased to 100, the vortices and particle entrapment in the cavities became unstable. Owing to the vortex movement in the cavities and additional eddy formation, no stable orbit was indicated around the primary vortex. These instabilities resulted in unstable particle trapping in the transitional flow regime; therefore, the particles departed from the cavity after several rotations. In most cases such trapping mode remains at Re = 100 – 200. In all the cases, at Re $>$ 500, the flow structure in the cavities satisfied the requirements for successful particle trapping [6,29]. Regardless the similar flow structure at Re = 100 and 1000 as presented in Figs. 3 and 4, the unstable flow structure observable in Figs. 7–14 plays a major role in efficient particle trapping Fluctuations observed in the cavities in this flow regime did not affect the particle trajectory owing to its low intensity and short living time, and the lift force [9] exerting on the particle primarily determined the particle path. However, owing to the three-dimensionality of the vortex, the particle was directed toward a parallel vertical plane, and the particle could not be further tracked using our equipment. This migration was more evident in longer cavities, where complex vortical structures have sufficient room to develop. Nevertheless, one can speculate that the particle remained entrapped in the recirculation zone, as particles escaping from the cavity in the middle plane were not observed. By contrast, the most stable particle path was observed in the triangular cavities at Re $>$ 500, which was similar to case of the rectangular and semicircular cavities at L/h = 1, where the vortex movement was restricted by the close proximity of the cavity side walls.

4. Conclusions

In this study, the flow structures in rectangular, semicircular, and triangular cavities with different L/h values of 1–4 for rectangular cavities and L/h = 1–2 for semicircular and triangular cavities in the range of Re = 10–1000 were investigated experimentally. Additionally, the behavior and trapping efficiency of 20 μm microparticles were analyzed.

Three distinctive flow regimes, namely attached, transitional, and separated, were observed in the cavities, based on the L/h and Re. The coarse threshold values obtained indicated the transfer between the flow regimes for each cavity type. Short rectangular and triangular cavities featured a stable recirculation zone because they were bounded by the side walls of the cavities, and only a small space was available for instability formation, which contribution to the flow structure is negligible.

The 20 μm diameter microparticles used accurately followed the streamlines in the cavity. The particles entered the cavity only after a recirculation zone was formed. To trap the particles effectively, the zone must be stable, and it is available at Re $>$ 100. Although, flow structure changes only slightly at Re $>$ 100, flow stability becomes the main defining parameter for efficient particle trapping. Trapping was the most stable in the triangular cavities, whereas in the rectangular and semicircular cavities, the particles migrated to parallel vertical planes. In triangular cavities vortex is bounded by the side walls and its movement and formation of instabilities are restricted; therefore, vortex is the most stable. The flow structure and particle behavior generalization, based on the geometry and flow regime, may facilitate the design of particle-trapping applications.

In this work qualitative results on particle trapping efficiency and its correlation with flow structure are presented. These results will serve as guidelines for continuing the research on a more quantitative level. In further research the influence of particle size and different cavities width will be performed to avoid the unfavorable effect of flow three-dimensionality to increase trapping efficiency at lower Re.

CRediT authorship contribution statement

Paulius Vilkinis: Conceptualization, Validation, Formal analysis, Investigation, Data curation, Writing – original draft, Writing – review & editing, Visualization. **Justas Šereika:** Investigation, Visualization, Writing – original draft, Writing – review & editing. **Gediminas Skarbalius:** Validation, Investigation. **Algis Džiugys:** Conceptualization, Formal analysis, Supervision. **Nerijus Pedišius:** Conceptualization, Resources, Supervision, Project administration.

Declaration of Competing Interest

The authors declare that they have no known competing financial interests or personal relationships that could have appeared to influence the work reported in this paper.

Data availability

Data will be made available on request.

Acknowledgments

This study was funded by the Research Council of Lithuania (grant number: S-MIP-21-21).

References

[1] H. Tavakoli, W. Zhou, L. Ma, S. Perez, A. Ibarra, F. Xu, S. Zhan, X.J. Li, Recent advances in microfluidic platforms for single-cell analysis in cancer biology, diagnosis and therapy, TrAC - Trends in Analytical Chemistry 117 (2019) 13–26, https://doi.org/10.1016/j.trac.2019.05.010.
[2] J. Yin, J. Deng, C. Du, W. Zhang, X. Jiang, Microfluidics-based approaches for separation and analysis of circulating tumor cells, TrAC -, Trends Anal. Chem. 117 (2019) 84–100, https://doi.org/10.1016/j.trac.2019.07.018.
[3] J. Nilsson, M. Evander, B. Hammarström, T. Laurell, Review of cell and particle trapping in microfluidic systems, Anal. Chim. Acta 649 (2009) 141–157, https://doi.org/10.1016/j.aca.2009.07.017.
[4] D. Di Carlo, Inertial microfluidics, Lab Chip 9 (2009) 3038, https://doi.org/10.1039/b912547g.
[5] S.C. Hur, A.J. Mach, D. Di Carlo, High-throughput size-based rare cell enrichment using microscale vortices, Biomicrofluidics 5 (2011) 022206, https://doi.org/10.1063/1.3576780.
[6] J. Zhou, S. Kasper, I. Papautsky, Enhanced size-dependent trapping of particles using microvortices, Microfluid. Nanofluidics. 15 (2013) 611–623, https://doi.org/10.1007/s10404-013-1176-y.
[7] A. Karimi, S. Yazdi, A.M. Ardekani, Hydrodynamic mechanisms of cell and particle trapping in microfluidics, Biomicrofluidics 7 (2013) 021501, https://doi.org/10.1063/1.4799787.
[8] M. Dhar, J. Wong, A. Karimi, J. Che, C. Renier, M. Matsumoto, M. Triboulet, E. B. Garon, J.W. Goldman, M.B. Rettig, S.S. Jeffrey, R.P. Kulkarni, E. Sollier, D. Di Carlo, High efficiency vortex trapping of circulating tumor cells, Biomicrofluidics 9 (2015), https://doi.org/10.1063/1.4937895.
[9] M. Jiang, S. Qian, Z. Liu, Fully resolved simulation of single-particle dynamics in a microcavity, Microfluid. Nanofluidics. 22 (2018) 144, https://doi.org/10.1007/s10404-018-2166-x.
[10] M. Khabiry, B.G. Chung, M.J. Hancock, H.C. Soundararajan, Y. Du, D. Cropek, W. G. Lee, A. Khademhosseini, Cell docking in double grooves in a microfluidic channel, Small 5 (2009) 1186–1194, https://doi.org/10.1002/smll.200801644.
[11] M. Bayareh, An updated review on particle separation in passive microfluidic devices, Chem. Eng. Process. - Process Intensif. 153 (2020) 107984, https://doi.org/10.1016/j.cep.2020.107984.

[12] L.L. Fan, X.K. He, Y. Han, L. Du, L. Zhao, J. Zhe, Continuous size-based separation of microparticles in a microchannel with symmetric sharp corner structures, Biomicrofluidics 8 (2014) 1–13, https://doi.org/10.1063/1.4870253.
[13] T.M. Faure, P. Adrianos, F. Lusseyran, L. Pastur, Visualizations of the flow inside an open cavity at medium range Reynolds numbers, Exp. Fluids 42 (2007) 169–184, https://doi.org/10.1007/s00348-006-0188-8.
[14] M. Cheng, K.C. Hung, Vortex structure of steady flow in a rectangular cavity, Comput. Fluids 35 (2006) 1046–1062, https://doi.org/10.1016/j.compfluid.2005.08.006.
[15] S.M. Grace, W.G. Dewar, D.E. Wroblewski, Experimental investigation of the flow characteristics within a shallow wall cavity for both laminar and turbulent upstream boundary layers, Exp. Fluids 36 (2004) 791–804, https://doi.org/10.1007/s00348-003-0761-3.
[16] Zeta Tak For Yu, Yi-Kuen LeVe, Man Wong, Y. Zohar, Fluid flows in microchannels with cavities, J. Microelectromechanical Syst. 14 (2005) 1386–1398, https://doi.org/10.1109/JMEMS.2005.859086.
[17] J. Šereika, P. Vilkinis, N. Pedišius, Analysis of cavity corner geometry effect on recirculation zone structure, Appl. Sci. 12 (2022), https://doi.org/10.3390/app12126288.
[18] R. Fishler, M.K. Mulligan, J. Sznitman, Mapping low-Reynolds-number microcavity flows using microfluidic screening devices, Microfluid. Nanofluidics. 15 (2013) 491–500, https://doi.org/10.1007/s10404-013-1166-0.
[19] C. Ozalp, A. Pinarbasi, B. Sahin, Experimental measurement of flow past cavities of different shapes, Exp. Therm Fluid Sci. 34 (2010) 505–515, https://doi.org/10.1016/j.expthermflusci.2009.11.003.
[20] H. Mercan, K. Atalık, Vortex formation in lid-driven arc-shape cavity flows at high Reynolds numbers, Eur. J. Mech. - B/Fluids. 28 (2009) 61–71, https://doi.org/10.1016/j.euromechflu.2008.02.001.
[21] F. Shen, M. Xu, Z. Wang, Z.M. Liu, Single-particle trapping, orbiting, and rotating in a microcavity using microfluidics, Appl. Phys Express 10 (2017), https://doi.org/10.7567/APEX.10.097301.
[22] D.S.W. Lim, J.P. Shelby, J.S. Kuo, D.T. Chiu, Dynamic formation of ring-shaped patterns of colloidal particles in microfluidic systems, Appl. Phys. Lett. 83 (2003) 1145–1147, https://doi.org/10.1063/1.1600532.
[23] H. Başağaoğlu, J.T. Carrola, C.J. Freitas, B. Başağaoğlu, S. Succi, Lattice Boltzmann simulations of vortex entrapment of particles in a microchannel with curved or flat edges, Microfluid. Nanofluidics. 18 (2015) 1165–1175, https://doi.org/10.1007/s10404-014-1509-5.
[24] F. Shen, P. Xiao, Z. Liu, Microparticle image velocimetry (μPIV) study of microcavity flow at low reynolds number, Microfluid. Nanofluidics. 19 (2015) 403–417, https://doi.org/10.1007/s10404-015-1575-3.
[25] J.Y. Park, M. Morgan, A.N. Sachs, J. Samorezov, R. Teller, Y. Shen, K.J. Pienta, S. Takayama, Single cell trapping in larger microwells capable of supporting cell spreading and proliferation, Microfluid. Nanofluidics. 8 (2010) 263–268, https://doi.org/10.1007/s10404-009-0503-9.
[26] W. Liu, C. Zheng, C.Y. Wu, Infiltration and resuspension of dilute particle suspensions in micro cavity flow, Powder Technol. 395 (2022) 400–411, https://doi.org/10.1016/j.powtec.2021.09.066.
[27] G. Guo, J. Gong, M. Zhang, Numerical investigation on flow characteristics of low-speed flow over a cavity with small aspect ratio, Int. J. Mech. Sci. 178 (2020) 105632, https://doi.org/10.1016/j.ijmecsci.2020.105632.
[28] F. Shen, S. Xue, B. Zhou, M. Xu, P. Xiao, Z. Liu, Evolution of single-particle recirculating orbits within a hydrodynamic microvortex, J. Micromechanics Microengineering. 28 (2018) 085018, https://doi.org/10.1088/1361-6439/aac02d.
[29] A. Volpe, C. Gaudiuso, A. Ancona, Sorting of particles using inertial focusing and laminar vortex technology: A review, Micromachines 10 (2019), https://doi.org/10.3390/mi10090594.